PAPER

Continuous enrichment of low-abundance cell samples using standing surface acoustic waves (SSAW)†

Q2

Yuchao Chen,[a] Sixing Li,[ab] Yeyi Gu,[c] Peng Li,[a] Xiaoyun Ding,[a] Lin Wang,[d] J. Philip McCoy,[e] Stewart J. Levine[e] and Tony Jun Huang[*ab]

Cell enrichment is a powerful tool in a variety of cellular studies, especially in applications with low-abundance cell types. In this work, we developed a standing surface acoustic wave (SSAW) based microfluidic device for non-contact, continuous cell enrichment. With a pair of parallel interdigital trans-ducers (IDT) deposited on a piezoelectric substrate, a one-dimensional SSAW field was established along disposable micro-tubing channels, generating numerous pressure nodes (and thus numerous cell-enrichment regions). Our method is able to concentrate highly diluted blood cells by more than 100 fold with a recovery efficiency of up to 99%. Such highly effective cell enrichment was achieved without using sheath flow. The SSAW-based technique presented here is simple, bio-compatible, label-free, and sheath-flow-free. With these advantages, it could be valuable for many biomedical applications.

Introduction

The ability to enrich cells or other biological samples with high viability and recovery efficiency is important in many applications in bioanalysis and medical diagnostics.[1–7] This ability is even more critical when dealing with low-abundance cell types (i.e., rare cells), such as circulating tumor cells, stem cells, and fetal cells.[8] Enrichment of these low-abundance cells is vital since higher sample concentration often leads to significantly improved signal-to-noise ratio in analysis. Conventional cell-enrichment techniques, such as centrifugation, are not suitable for use with these low-abundance cell types due to the significant loss of cell viability and limited ability to handle small quantities of cells with high recovery efficiency. In this regard, microfluidic-based approaches have significant advantages. Unlike the traditional macroscale platforms, parameters in microfluidic devices (e.g., channel dimensions, flow profile) can be precisely controlled at the cellular scale; this precise control facilitates high capture efficiency and isolation

purity.[9,10] Furthermore, enriched cells can be quickly and precisely manipulated to next-stage analysis (e.g., genomic analysis, drug screening) or on-chip cell culturing as part of an integrated and automated process, eliminating the inter-mediate procedures required in macro-scale systems.[11,12]

Among all the microfluidic-based cell-enrichment tech-niques, those using non-contact cell trapping are often pre-ferred due to their ability to limit surface interaction and mechanical stress on cells and provide convenient sample transfer.[13,14] Non-contact cell trapping is usually achieved by applying external forces to the cells to counteract the viscous drag force in continuous flows. Over the past decades, various on-chip techniques have been implemented to trap cells or micro-particles in microfluidic flows, including dielectrophoresis (DEP),[15–17] optical tweezers,[18–20] and magnetic tweezers.[21,22] Recently, acoustic-based approaches[23–29] have received signifi-cant attention because of their versatility, bio-compatibility, and label-free, non-contact nature. For example, the standing surface acoustic wave (SSAW) based microfluidic techniques have resulted in a variety of applications (e.g., cell/particle focusing, patterning, separation, and sorting).[30–40] Recently, our group demonstrated a SSAW-based cell patterning tech-nique that can trap cells or microparticles in stationary fluids.[41,42] However, SSAW-based cell trapping in moving fluids for on-site sample enrichment has not yet been demonstrated.

In this work, we demonstrate a SSAW-based cell trapping and enrichment technique that operates in continuous flows. Our experimental results indicate that this SSAW-based cell enrichment technique can achieve a recovery efficiency of more than 90% for highly diluted blood cells and concentrate

[a] Department of Engineering Science and Mechanics, The Pennsylvania, State University, University Park, PA, 16802, USA. E-mail: junhuang@psu.edu
[b] Cell and Developmental Biology (CDB) Graduate Program, The Huck Institutes of the Life Sciences, The Pennsylvania State University, University Park, PA 16802, USA
[c] Department of Food Science, The Pennsylvania State University, University Park, PA, 16802, USA
[d] Ascent Bio-Nano Technologies, Inc., State College, PA, 16802, USA
[e] National Heart, Lung, and Blood Institute, NIH, Bethesda, MD 20892, USA
† Electronic supplementary information (ESI) available: Including videos of sample enrichment at the entrance and exit of enrichment region, and multi-channel sample enrichment. See DOI: 10.1039/c3lc51001h

the sample by a factor of 100–1000. Experimental results indicate excellent post-enrichment cell viability. Moreover, detachable microchannels enabled by coupling gel allow simultaneous multichannel processing to enhance the enrichment efficiency. Our SSAW-based device is simple to fabricate and highly flexible in terms of channel material selection, resulting in significant potential for system integration and mass production. With its high recovery efficiency, bio-compatibility, and simplicity, the SSAW-based cell enrichment approach presented here can be valuable in many cell-based bioanalytical systems.[43–50]

Working mechanism

Fig. 1A shows the schematic of the SSAW-based cell enrichment device. A pair of parallel interdigital transducers (IDTs) was deposited onto the lithium niobate (LiNbO$_3$) substrate. A micro-tubing channel with spherical cross-sections was assembled in the SSAW-activated region of the substrate with its long axis oriented in the propagation direction of acoustic waves. In order for the acoustic waves to propagate into the microchannel, a coupling gel was used to fill the gap between the tubing and the substrate, as shown in Fig. 1B. Applying an AC signal to the IDTs results in the generation of a SSAW field and thus the creation of a non-uniform pressure field in the fluid with a periodic distribution of pressure nodes (*i.e.*, minimum pressure amplitude) and antinodes (*i.e.*, maximum pressure amplitude). In the presence of the SSAW field, a cell suspension was injected into the microchannel. Upon entering the region where the coupling gel bonds the microchannel to

Fig. 1 (A) Schematic of the SSAW-based sample enrichment device. Two parallel IDTs generate a SSAW field to trap cells inside the microchannel. (B) Cross-sectional view of the microdevice in the *y*–*z* plane. A coupling gel is coated between the tubing and the piezoelectric substrate. (C) Mechanism of SSAW-based cell trapping for enrichment in continuous flows. The dashed lines indicate the pressure distribution in the microchannel. The arrows on the cells indicate the direction of cell movement.

the substrate, known as the enrichment region, cells were trapped at SSAW pressure nodes. As more fluid passed through the enrichment region, the concentration of the trapped cells gradually increased until the trapping was saturated. Finally, the SSAW was turned off to release the cells. The enriched sample could be collected from the outlet of the microchannel or directly delivered into the downstream for further analysis and processing.

When cells enter the pressure field, they experience two forces in the *x*–*y* plane: the primary acoustic radiation force (F_r) and the viscous drag force (F_v), which can be expressed as[51]

$$F_r = -\left(\frac{\pi p_0^2 V_p \beta_m}{2\lambda}\right)\phi(\beta,\rho)\sin\left(\frac{4\pi x}{\lambda}\right) \quad (1)$$

$$\phi = \frac{5\rho_p - 2\rho_m}{2\rho_p + \rho_m} - \frac{\beta_p}{\beta_m} \quad (2)$$

$$F_v = -6\pi\eta r v \quad (3)$$

where p_0, V_p, λ, ϕ, x, ρ_m, ρ_p, β_m, β_p, η, r, and v are pressure amplitude, particle volume, SSAW wavelength, contrast factor, distance from the pressure node, density of medium, density of cells, compressibility of medium, compressibility of cells, medium viscosity, cell radius, and relative velocity, respectively. As shown in Fig. 1C, the primary radiation force moves the particles to the pressure nodes. As the distance between particles decreases, the secondary radiation force plays a dominant role in aggregating particles together and forming an array of clusters.[15] The component of the primary force along the *x* axis immobilizes the clusters in the pressure nodes by competing with the viscous drag force in the opposite direction. The clusters continue to attract nearby particles, growing in size and resulting in an increase in radiation forces on clusters. Because each pressure node has a maximum trapping capacity, the saturation occurs gradually from the upstream end to the downstream end of the enrichment region. When the volume of a trapped cluster is saturated, some particles will be flushed off and trapped again at the downstream pressure nodes.

Materials and methods

We used Y+128° X-propagation LiNbO$_3$ as a piezoelectric substrate to generate SSAW. The IDTs were fabricated through standard photolithography processes.[32] After depositing a metal double layer (Cr/Au, 50 Å/500Å) with an e-beam evaporator (Semicore Corp), two parallel IDTs were formed on the LiNbO$_3$ substrate by a lift-off process. The IDTs we designed had 20 pairs of electrodes with consistent electrode widths and spacing gaps (50 μm). Both IDTs could generate identical surface acoustic waves (SAWs) with a wavelength of 200 μm at a resonance frequency of 19.6 MHz. Coherent AC signals, which were generated by an RF signal generator (Agilent
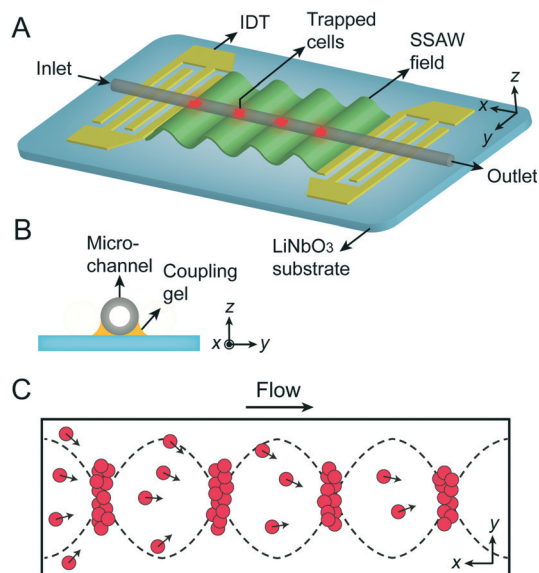
Tech, E4422B) and amplified with a power amplifier (Amplifier Research, 100A250A), were applied to both IDTs to generate two travelling SAWs along the delay line, forming a one-dimensional (1D) SSAW field. The device was immobilized on the stage of an inverted microscope (Nikon TE2000U). A CCD camera (CoolSNAP HQ2, Photometrics, Tucson, AZ) was connected to the microscope to record the cell-enrichment process. The fluorescence intensity was analyzed with ImageJ 1.46 software.

In the experiments, we used polyethylene tubing (BD, Franklin Lakes, NJ) with an inner diameter of 280 μm as a microchannel. The micro tubing was assembled at the SAW-activated region of the LiNbO$_3$ substrate with its long axis oriented in the direction of SAW propagation (Fig. 1A). The center of the SSAW-activated region was coated with a KY gel (Johnson & Johnson, New Brunswick, NJ) between the substrate and the microchannel (Fig. 1B). The coupling length was about 5 mm. A syringe pump (neMESYS, Cetoni GmbH, Korbussen, Germany) was used to control the flow rate. Each sample collected from the outlet was subsequently diluted into a proper volume, and counted in a hemacytometer (Hausser Scientific, Horsham, PA) three times. For the highly diluted blood samples (10^3 cells mL^{-1}), the number of trapped cells was directly counted in the microchannel through the microscope.

Fluorescent microspheres (Dragon green, 480/520, Bangs laboratories Inc, Fishers, IN) were used to characterize the device. Microspheres with a diameter of 7 μm were suspended in 1% SDS solution at a concentration of 10^6 particles mL^{-1}. Human whole blood purchased from Zen-bio, Inc. was diluted with 1× PBS solution into different concentrations (10^3–10^5 cells mL^{-1}) for cell enrichment. Since it was not able to culture red blood cells, cell viability was tested in a Murine Raw 264.7 macrophage cell line. Cells were either treated by passing through a microchannel with or without SSAW enrichment, or incubated at 65 °C for 15 min. Cells without any treatment and culture medium were used as a positive and a negative control, respectively. After treatment, cells were seeded in a 96-well plate in a complete Dulbecco's modified Eagle's medium (DMEM, Invitrogen) containing 10% (v/v) fetal bovine serum (Atlanta Biologicals) and 1% (v/v) penicillin–streptomycin (Cellgro) at a density of 10^5 cells mL^{-1}. After 24 h, cell viability was determined by MTT assay[52] and its absorbance at 450 nm was expressed as mean ± standard deviation of five experimental measurements.

Results and discussion

SSAW-based particle trapping

The coupling gel between the microchannel and piezoelectric substrate allows acoustic waves to propagate into the fluids in the microchannel and generate a non-uniform pressure distribution. In our design, the length of the enrichment region is about 5 mm and the distance between each adjacent pressure node is 100 μm (half wavelength). The number of pressure nodes (trapping positions) created in the microchannel is approximately 50, providing a high trapping capacity. Fig. 2
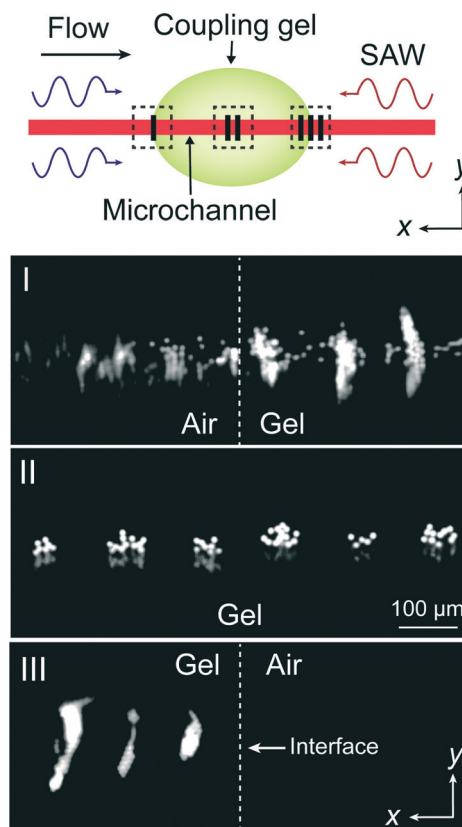

Fig. 2 Recorded fluorescent images at (I) the entrance, (II) the center, and (III) the exit of the enrichment region, respectively. I, II, and III indicate the observation locations during enrichment. The white dashed lines indicate the boundaries of the enrichment region.

shows the fluorescent images of the particles trapped along different locations of the enrichment region. In the entrance of enrichment region (Fig. 2-I), a comparison between the air medium (non-enrichment region) and the gel medium (enrichment region) is presented. After the SSAW field was applied, fluorescent polystyrene beads flowed into the trapping region and aggregated at the pressure nodes. The particles which had not entered the enrichment region experienced no acoustic radiation force and remained randomly distributed in the microchannel. Fig. 2-II shows that particles placed in the middle of the enrichment region were well patterned by the acoustic radiation forces. While the power was on, all of the particles remained inside the enrichment region as shown in Fig. 2-III. Even though continuous flows were applied, no particle was observed in the lower reaches of the microchannel (outside the trapping region), indicating effective particle trapping by SSAW (see ESI† Video 1).

Device characterization

We used fluorescent beads to characterize the process of sample enrichment. As illustrated in Fig. 3A, this process has three stages: enrichment, saturation, and release. Fig. 3B shows typical images of each stage (see ESI† Video 2 and Video 3). Before SSAW was turned on, particles passed through the detection
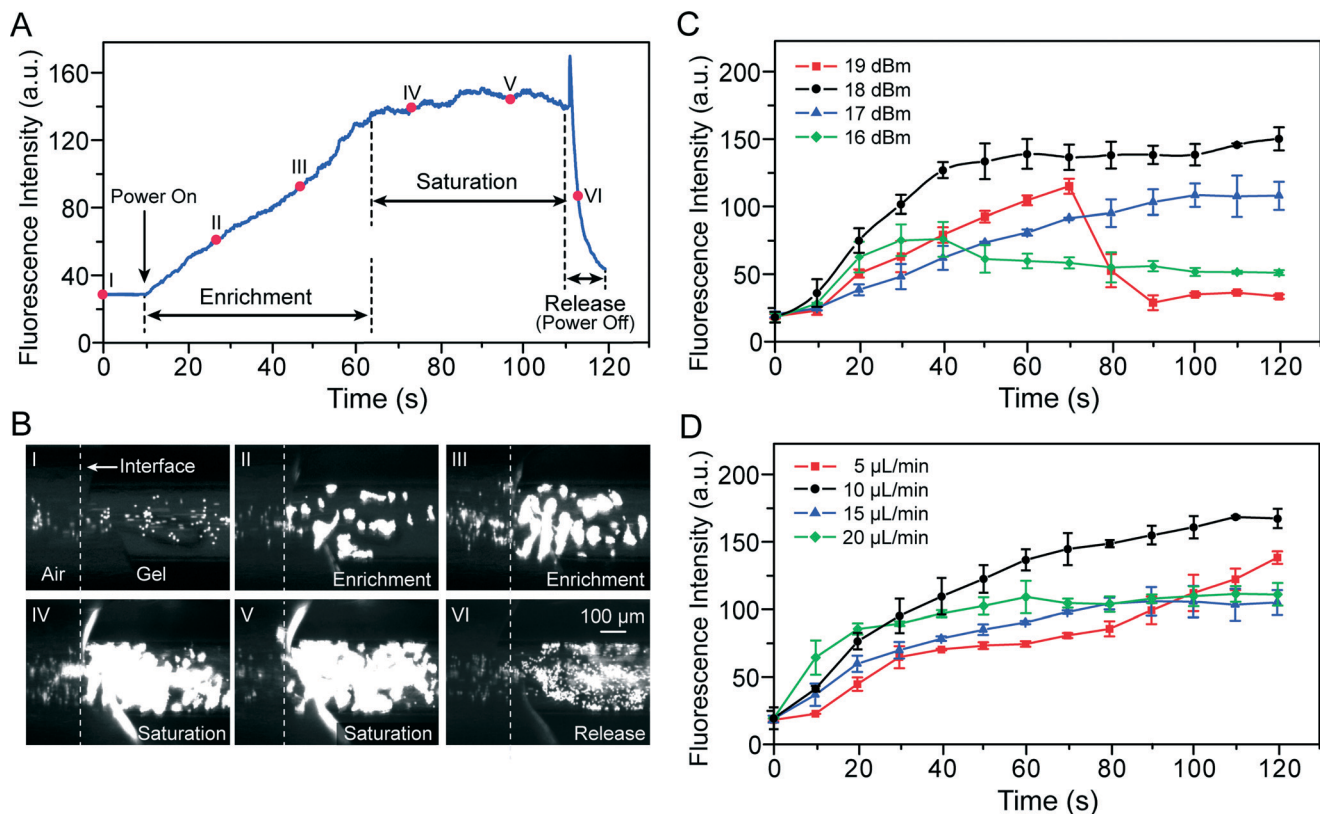
Fig. 3 (A) The sample enrichment process presented as variation in the fluorescence intensity. I–VI indicate six specific points of time during the process. (B) Recorded fluorescent images of the enrichment-region entrance at the points of time (I–VI) indicated in (A). The influence of different (C) input powers and (D) flow rates on SSAW-based sample enrichment. The error bars denote the standard deviation of three experimental measurements.

region at a consistent velocity (Fig. 3B-I), resulting in little change of the fluorescence intensity. The intensity started to increase as soon as a SSAW field was applied. The growth rate was approximately linear because the acoustic radiation force captured most of the particles once they entered the trapping region. During this period (the enrichment stage), the sample was gradually enriched inside the enrichment region (Fig. 3B-II and III). When the trapped sample approached the maximum capacity of the pressure node, some trapped particles were released and new particles were trapped achieving dynamic equilibrium and retaining a constant amount of particles in the pressure node (Fig. 3B-IV and V). This saturation stage started with a sharp decrease in the growth rate of the fluorescence intensity. During saturation, the intensity was maintained at a certain level (~150 in this case) with small fluctuations, as shown in Fig. 3A. The stable immobilization of sample inside the microchannel allowed for the introduction of a washing buffer as an additional purification step. The purification step is useful to remove contaminated molecules and exchange mediums, an important process in online biochemical analysis.[22] As soon as the SSAW was turned off, the fluorescence intensity experienced an immediate jump (a sharp peak in Fig. 3A) since a large amount of the fluorescent beads were released and simultaneously passed through the detection region. The particles were removed by the flow (Fig. 3B-VI), leading to a fast decay of the fluorescence intensity.

We further studied the influence of input power on enrichment ability, as shown in Fig. 3C. Four power levels from 16 to 19 dBm were used to enrich the particles at a single flow rate. When the input power was tuned from 16 to 18 dBm, the fluorescence intensity at the saturation stage increased from ~50 to ~150, indicating that a higher trapping capacity was achieved due to stronger acoustic radiation forces. Though a higher input power resulted in a higher pressure amplitude (p_0) and thus stronger acoustic radiation forces exerted on the particles according to eqn (1), acoustic streaming also became obvious at higher power levels (19 dBm and above).[53] Fluorescence intensity grew linearly during the first 70 s but then suddenly dropped to the original level in the next 10 s. This was because the acoustic streaming became dominant and particles failed to remain trapped at the pressure nodes.

The flow rate is another factor that influences the sample enrichment. To trap particles at the pressure nodes, the acoustic radiation forces (F_r) should be larger than the viscous drag forces (F_v). A higher flow rate could help to enhance throughput, but also exerts larger viscous drag forces on particles due to the higher particle velocity (v) in eqn (3), leading to a decrease in the recovery efficiency. We conducted sample enrichment with four different flow rates and a constant input power of 18 dBm. As shown in Fig. 3D, a flow rate of 5 µL min^{-1} achieved a smaller growth rate in

fluorescence intensity than 10 μL min^{-1}, since the smaller flow velocity of the particles induced a lower speed of sample accumulation. However, when flow rates of 15 and 20 μL min^{-1} were used, the saturated fluorescence intensity decreased by approximately 42% as compared to the flow rate of 10 μL min^{-1}. At a higher flow rate, the stronger viscous drag forces enable particles to escape trapping by acoustic radiation forces.

Parallel sample enrichment

Polydimethylsiloxane (PDMS) has been widely used in SAW microfluidics for the fabrication of predesigned microchannels, which can then be bonded to a piezoelectric substrate to form a SSAW-based microdevice. However, the relatively high cost of the piezoelectric substrate limits the device's utility in disposable applications. In our work, polyethylene micro tubings were assembled onto the LiNbO$_3$ substrate as microchannels. After each run, the used tubings could be easily peeled off and replaced by new tubings to avoid cross-contamination. In addition to disposability, the micro tubings enable a multichannel, SSAW-based sample enrichment configuration with our device. The parallel sample enrichment could help to improve the working efficiency and throughput by enriching more cells in less time, or enriching different species of cells simultaneously. As shown in Fig. 4A, by assembling an array of micro-tubing channels (three in this case) onto the piezoelectric substrate, parallel sample enrichment was conveniently established. In each channel, the efficiency of the
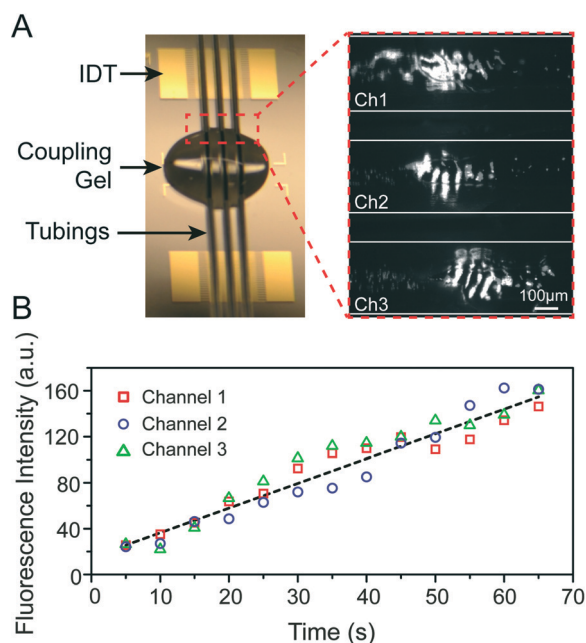
sample enrichment was consistent (Fig. 4B), revealing a steady performance of each working unit.

Enrichment of highly diluted blood cells

Serially diluted human whole blood was used as a sample for cell enrichment to demonstrate the capability of our device. Blood cells with three concentrations (10^5, 10^4, and 10^3 cells mL^{-1}) were studied in the experiments. Each sample was enriched for 10 min at a flow rate of 7 μL min^{-1}. The enrichment process is shown in Fig. 5A. The blood cells gradually accumulated at the pressure nodes once they entered the enrichment region, resulting in growth of cell clusters. Since the cell samples were highly diluted, trapping saturation did not occur during the enrichment process. The recovery efficiency for the enrichment of diluted blood cells was calculated and shown in Fig. 5B. The recovery efficiency was defined as the ratio of measured cell concentration to the theoretical 100%-recovered concentration. A recovery efficiency of 93.1 ± .9% and 97.3 ± 5.2% was obtained when diluting the blood sample to 10^5 cells mL^{-1} and 10^4 cells mL^{-1}, respectively. When the blood sample was further diluted to a concentration of 10^3 cells mL^{-1}, 99.1 ± 11.3% of the blood cells could be recovered. Since the volume of the enrichment region was about 0.3 μL (5 mm in length, 0.28 mm in diameter), after running for 10 min with a flow rate of 7 μL min^{-1}, 70 μL of the sample was enriched into a final volume of 0.3 μL with a recovery efficiency more than 90%, indicating that the sample was concentrated by two orders of magnitude. The concentration factor could be further increased with an increase in processed sample volume. As a result, the concentration of
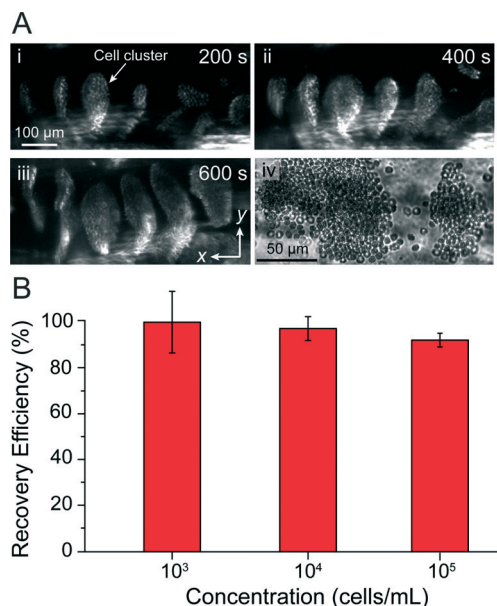

Fig. 4 (A) SSAW-based parallel sample enrichment by assembling multiple micro-tubing channels onto the piezoelectric substrate. Right lane shows the fluorescent image of simultaneous sample enrichment in three microchannels (see ESI† Video 4). (B) Performance of parallel sample enrichment in three microchannels presented as fluorescence intensity.

Fig. 5 (A) i–iii: Dynamic process of blood cell enrichment. The images were taken in 200 s interval for 600 s. iv: Magnified image of cell clusters. (B) Recovery efficiency of cell enrichment at different concentrations. The error bars denote the standard deviation of three experimental measurements.

the sample after enrichment could be enhanced up to 100–1000 times, which shows an improvement over many other cell or particle enrichment techniques (typical concentration factor: <100 times).[54–60]

Cell viability test

One of the biggest advantages of our SSAW-based cell enrichment technique is its bio-compatibility. In this regard, we measured the viability of cells after SSAW enrichment by MTT assay. Cells without any treatment and culture medium were used as a positive and a negative control, respectively. As shown in Fig. 6, the viability of cells which passed through the channel with and without SSAW enrichment was measured to be at the same level as the positive control (between 0.25 and 0.30), while the viability of the cells incubated at 65 °C for 15 min was close to the value of culture medium (lower than 0.10), indicating that the process of SSAW-based enrichment had no significant effect on cell viability. Though the viabilities of cells passing through the channel with and without SSAW enrichment (the second and third bars in Fig. 6) were observed to be different, the P values between these two groups and the positive control (the first bar) were calculated to be 0.9204 and 0.3108, both of which are larger than 0.05. As a result, the difference of these three groups could be considered to be insignificant.

Conclusions

By applying a SSAW field to induce a non-uniform pressure distribution in the microfluidic channel, a large number of
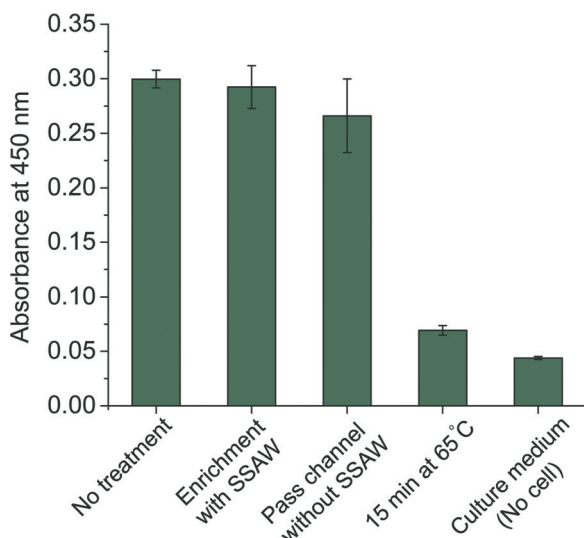

Fig. 6 Cell viability test. Murine Raw 264.7 macrophages were either treated by passing through a microchannel with or without SSAW enrichment, or incubated at 65 °C for 15 min. Cells without any treatment and culture medium were used as a positive and a negative control, respectively. After treatment, cells were seeded in a 96-well plate for 24 h, and cell viability was determined by MTT assay and expressed as mean ± standard deviation of three experimental measurements.

pressure nodes can be generated to trap cells for sample enrichment. This SSAW-based technique allows the enrichment of highly-diluted cell samples with excellent performance (concentration factor: 100–1000; recovery efficiency: over 90%; high viability). In addition, the gel-coupling method provides further advantages: flexibility in the channel materials, simple fabrication, and high-throughput parallel sample enrichment. These advantages make the SSAW-based technique presented here promising in the enrichment of low-abundance rare cells for cellular study.

Acknowledgements

References

1 S. Zheng, H. K. Lin, B. Lu, A. Williams, R. Datar, R. J. Cote and Y.-C. Tai, *Biomed. Microdevices*, 2011, **13**, 203–213.
2 G. M. Whitesides, *Nature*, 2006, **442**, 368–373.
3 P. Neuzil, S. Giselbrecht, K. Länge, T. J. Huang and A. Manz, *Nat. Rev. Drug Discovery*, 2012, **11**, 620–632.
4 X. Mao and T. J. Huang, *Lab Chip*, 2012, **12**, 1412–1416.
5 X. Mao and T. J. Huang, *Lab Chip*, 2012, **12**, 4006–4009.
6 Y. T. Kim, Y. Chen, J. Y. Choi, W.-J. Kim, H.-M. Dae, J. Jung and T. S. Seo, *Biosens. Bioelectron.*, 2012, **33**, 88–94.
7 Y. Chen and T. S. Seo, *Electrophoresis*, 2011, **32**, 1456–1464.
8 P. Li, Z. S. Stratton, M. Dao, J. Ritz and T. J. Huang, *Lab Chip*, 2013, **13**, 602–609.
9 S. C. Hur, A. J. Mach and D. DiCarlo, *Biomicrofluidics*, 2011, **5**, 022206.
10 S. C. Hur, N. K. Henderson-MacLennan, E. R. B. McCabec and D. DiCarlo, *Lab Chip*, 2011, **11**, 912–920.
11 W. C. Chang, L. P. Lee and D. Liepmanna, *Lab Chip*, 2005, **5**, 64–73.
12 J. A. Phillips, Y. Xu, Z. Xia, Z. H. Fan and W. Tan, *Anal. Chem.*, 2009, **81**, 1033–1039.
13 J. Nilsson, M. Evander, B. Hammarström and T. Laurell, *Anal. Chim. Acta*, 2009, **649**, 141–157.
14 M. Evander and J. Nilsson, *Lab Chip*, 2012, **12**, 4667–4676.
15 S. Park, Y. Zhang, T.-H. Wang and S. Yang, *Lab Chip*, 2011, **11**, 2893–2900.
16 N. Gadish and J. Voldman, *Anal. Chem.*, 2006, **78**, 7870–7876.
17 D. Chen and H. Du, *Microfluid. Nanofluid.*, 2010, **9**, 281–291.
18 D. G. Grier, *Nature*, 2003, **424**, 810–816.
19 C. Piggee, *Anal. Chem.*, 2009, **81**, 16–19.
20 L. Mitchem and J. P. Reid, *Chem. Soc. Rev.*, 2008, **37**, 756–769.

21 H. Lee, A. M. Purdon, V. Chu and R. M. Westervelt, *Nano Lett.*, 2004, **4**, 995–998.

22 M. T. Bryan, K. H. Smith, M. E. Real, M. A. Bashir, P. W. Fry, P. Fischer, M.-Y. Im, T. Schrefl, D. A. Allwood and J. W. Haycock, *IEEE Magn. Lett.*, 2010, **1**, 1500104.

23 B. Hammarström, M. Evander, H. Barbeau, M. Bruzelius, J. Larsson, T. Laurell and J. Nilssona, *Lab Chip*, 2010, **10**, 2251–2257.

24 J. Svennebring, O. Manneberg, P. Skafte-Pedersen, H. Bruus and M. Wiklund, *Biotechnol. Bioeng.*, 2009, **103**, 323–328.

25 O. Manneberg, B. Vanherberghen, B. Önfelt and M. Wiklund, *Lab Chip*, 2009, **9**, 833–837.

26 J. V. Norris, M. Evander, K. M. Horsman-Hall, J. Nilsson, T. Laurell and J. P. Landers, *Anal. Chem.*, 2009, **81**, 6089–6095.

27 M. Evander, L. Johansson, T. Lilliehorn, J. Piskur, M. Lindvall, S. Johansson, M. Almqvist, T. Laurell and J. Nilsson, *Anal. Chem.*, 2007, **79**, 2984–2991.

28 L. Johansson, M. Evander, T. Lilliehorn, M. Almqvist, J. Nilsson, T. Laurell and S. Johansson, *Ultrasonics*, 2013, **53**, 1020–1032.

29 M. Wiklund, P. Spégel, S. Nilsson and H. M. Hertz, *Ultrasonics*, 2003, **41**, 329–333.

30 S. Li, X. Ding, F. Guo, Y. Chen, M. I. Lapsley, S.-C. S. Lin, L. Wang, J. P. McCoy, C. E. Cameron and T. J. Huang, *Anal. Chem.*, 2013, **85**, 5468–5474.

Q4 31 X. Ding, S.-C. S. Lin, B. K., H. Yue, S. Li, J. Shi, S. J. Benkovic and T. J. Huang, *Proc. Natl. Acad. Sci. U. S. A.*, 2012, **109**, 11105–11109.

32 J. Shi, H. Huang, Z. Stratton, A. Lawit, Y. Huang and T. J. Huang, *Lab Chip*, 2009, **9**, 3354–3359.

33 J. Shi, X. Mao, D. Ahmed, A. Colletti and T. J. Huang, *Lab Chip*, 2008, **8**, 221–223.

34 Y. Chen, X. Ding, S.-C. S. Lin, S. Yang, P.-H. Huang, N. Nama, Y. Zhao, A. A. Nawaz, F. Guo, W. Wang, Y. Gu, T. E. Mallouk and T. J. Huang, *ACS Nano*, 2013, **7**, 3306–3314.

35 X. Ding, P. Li, S.-C. S. L., Z. S. Stratton, N. Nama, F. Guo, D. Slotcavage, X. Mao, J. Shi, F. Costanzo and T. J. Huang, *Lab Chip*, 2013, **13**, 3626–3649.

36 X. Ding, S.-C. S. Lin, M. I. Lapsley, S. Li, X. Guo, C. Y. K. Chan, I.-K. Chiang, J. P. McCoy and T. J. Huang, *Lab Chip*, 2012, **12**, 4228–4231.

37 J. Shi, S. Yazdi, S.-C. S. Lin, X. Ding, I.-K. Chiang, K. Sharp and T. J. Huang, *Lab Chip*, 2011, **11**, 2319–2324.

38 S.-C. S. Lin, X. Mao and T. J. Huang, *Lab Chip*, 2012, **12**, 2766–2770.

39 J. Nam, Y. Lee and S. Shin, *Microfluid. Nanofluid.*, 2011, **11**, 317–326.

40 Q. Zeng, H. W. L. Chan, X. Z. Zhao and Y. Chen, *Microelectron. Eng.*, 2010, **87**, 1204–1206.

41 J. Shi, D. Ahmed, X. Mao, S.-C. S. Lin and T. J. Huang, *Lab Chip*, 2009, **9**, 2890–2895.

42 X. Ding, J. Shi, S.-C. S. Lin, S. Yazdi, B. Kiraly and T. J. Huang, *Lab Chip*, 2012, **12**, 2491–2497.

43 N. Pamme and A. Manz, *Anal. Chem.*, 2004, **76**, 7250–7256.

44 W. Chen, S. Weng, F. Zhang, S. Allen, L. Bao, R. H.-W. Lam, J. A. Macoska, S. D. Merajver and J. Fu, *ACS Nano*, 2013, **7**, 566–575.

45 S. Park, Y Zhang, T. H. Wang and S. Yang, *Lab Chip*, 2011, **11**, 2893–2900.

46 Y. Zhou, Y. Pang and Y. Huang, *Anal. Chem.*, 2012, **84**, 2576–2584.

47 Y. Zhang, S. Park, S. Yang and T. H. Wang, *Biomed. Microdevices*, 2010, **12**, 1043–1049.

48 G. B. Salieb-Beugelaar, G. Simone, A. Arora, A. Philippi and A. Manz, *Anal. Chem.*, 2010, **82**, 4848–4864.

49 N.-T. Huang, W. Chen, B. Oh, T. T. Cornell, T. P. Shanley, J. Fu and K. Kurabayashi, *Lab Chip*, 2012, **12**, 4093–4101.

50 C. Zheng, J. Wang, Y. Pang, J. Wang, W. Li, Z. Ge and Y. Huang, *Lab Chip*, 2012, **12**, 2487–2490.

51 K. Yosioka and Y. Kawasima, *Acustica*, 1955, **5**, 167–173.

52 J. van Meerloo, G. J. Kaspers and J. Cloos, *Methods Mol. Biol.*, 2011, **731**, 237–245.

53 R. P. Hodgson, M. K. Tan, L. Y. Yeo and J. R. Friend, *Appl. Phys. Lett.*, 2009, **94**, 024102.

54 H. Moncada-Hernández and B. H. Lapizco-Encinas, *Anal. Bioanal. Chem.*, 2010, **396**, 1805–1816.

55 J. J. Hawkes and W. T. Coakley, *Enzyme Microb. Technol.*, 1996, **19**, 57–62.

56 M. Yamada and M. Seki, *Anal. Chem.*, 2006, **78**, 1357–1362.

57 R. Kwak, S. J. Kim and J. Han, *Anal. Chem.*, 2011, **83**, 7348–7355.

58 D. Puchberger-Enengl, S. Podszun, H. Heinz, C. Hermann, P. Vulto and G. A. Urban, *Biomicrofluidics*, 2011, **5**, 44111.

59 J. Warrick, B. Casavant, M. Frisk and D. Beebe, *Anal. Chem.*, 2010, **82**, 8320–8326.

60 A. J. Mach, J. H. Kim, A. Arshi, S. C. Hur and D. DiCarlo, *Lab Chip*, 2011, **11**, 2827–3016.